

Chapter 15

Grain Boundary Networks

Bryan W. Reed and Christopher A. Schuh

15.1 Introduction

Statistical information about grain orientations within a polycrystal has been available to materials researchers for many decades. In particular, the orientation distribution, or crystallographic texture information, has been measured using X-ray diffraction techniques since about 1950. Consequently, the role of texture in materials performance and design is widely appreciated and commonly taught in the core Materials Science curriculum. However, texture data represent only “one-point” statistics, and do not capture microstructural geometry or topology.

The landmark achievement of EBSD was the ability not only to measure crystal orientations, but to map them spatially. This technology dramatically expanded the amount of statistical information available about microstructures. Notably, the one-point distribution of grain orientations can be expanded to include two-point, three-point, or higher-order correlations among grain orientations; we may construct not only distributions of orientations, but of pairs or triplets of them, for example. Indeed, so overwhelming is the possible space of statistical information available from a single EBSD dataset that the field has yet to develop common techniques and tools for managing and analyzing it. This will remain an active area of materials research for the foreseeable future.

EBSD provides two broad classes of combined orientation and spatial information. First, traditional geometrical aspects of the grain structure, such as grain size and shape distributions, can not only be measured from EBSD data, but augmented by local grain-specific knowledge of their orientation. This information may be used to predict or understand, e.g., volumetrically averaged bulk properties such as effective elastic constants. The use of EBSD data in these applications is discussed elsewhere in this volume (see Chapters 12 and 13).

Second, the coverage of a large section of microstructure with EBSD permits study of the topological aspects of the microstructural elements, and connectivity among elements related by their orientations or crystallography. For example, clusters of grains related by specific misorientations, or networks of grain boundaries of related symmetries can be identified and quantified using, e.g., neighbor distribution information, number of faces per grain, or distributions of branching features such as triple junctions and quadruple nodes. These elements of the microstructure tend to be especially relevant for properties involving path dependence, as for transport or damage propagation across a specimen. Such topological issues of microstructure, and their analysis with EBSD, are the focus of this chapter.

Concurrently with—and spurred by—the development of EBSD, materials scientists have increasingly focused attention on the importance of microstructural topology in governing materials properties. Examples in this regard include the development of polycrystalline high- T_c superconductors, in which a network of grains related by low-angle misorientations is required to pass supercurrent, or grain-boundary engineered metals that resist intergranular damage propagation

B.W. Reed (✉)
Lawrence Livermore National Laboratory, Livermore,
CA 94550, USA
e-mail: reed12@llnl.gov

by incorporating a high fraction of “special” damage resistant grain boundaries (Frary and Schuh 2003b; Gaudett and Scully 1994; Krupp et al. 2005; Randle 2004; Schuh et al. 2003a; Schwartz et al. 2006; Wells et al. 1989). This shift in focus has also led to the integration of statistical physics concepts into materials science, including notions borrowed from percolation theory and network science (Basinger et al. 2005; Bouchaud 1997; Fullwood et al. 2006; McGarrity et al. 2005; Meinke et al. 2003; Nichols et al. 1991a, 1991b; Romero et al. 1996; Schuh and Frary 2006; Schuh et al. 2003c; Van Siclen 2006; Wells et al. 1989). This represents a potentially revolutionary paradigm for materials design, as the “universal” concepts from statistical physics may unify our view of disparate materials and properties.

In the following sections, we briefly review some of the local microstructural elements that are amenable to analysis and quantification by EBSD, and progress to the study of their connectivity and topological characteristics. We then address the issue of connecting these microstructural measures with properties, and conclude with some comments on the frontier areas of research in this field.

15.2 Measurement and Classification of Local Network Elements

15.2.1 General Definitions for Single Boundaries

In specifying the mathematical elements of a grain boundary network, we will start with some definitions. A *grain* is a contiguous three-dimensional region consisting of a single phase with a crystalline orientation constant to within some tolerance (typically $\sim 1\text{--}2^\circ$ for a well-annealed polycrystal), while a *grain boundary* is a contiguous two-dimensional region where two grains meet. This definition of grains does not distinguish between grains and subgrains; what would often be called a twin subgrain of a larger grain is considered here to be a separate grain.

Two-dimensional cross sections of grains, and the corresponding one-dimensional cross sections of grain boundaries with triple junctions at their end points, are easy to identify in high-quality EBSD data sets. The

tolerance is typically set to be compatible with the point-to-point experimental uncertainty in the orientation, which varies with the signal-to-noise ratio in the measurement. Transitivity is usually enforced, i.e., if pixels A and B belong to the same grain, and B and C belong to the same grain, then so do A and C, even if the misorientation between A and C exceeds the tolerance. This avoids the situation represented in Fig. 15.1. As a result, boundary identification algorithms never find isolated boundaries nor boundaries that abruptly end in the middle of grains; all boundaries end either at triple junctions or at the edge of the measured region. Various algorithms exist for identifying and dropping out single-pixel noise, and it is highly recommended that these be applied prior to any grain boundary network analysis, lest single-pixel grains dominate the statistics. A simple method is to identify pixels that (1) have poor signal quality and (2) are surrounded by pixels of significantly different orientation, and then to overwrite each such pixel with the orientation from its best-quality neighbor.

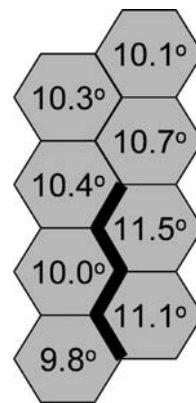


Fig. 15.1 An example of what it means to enforce transitivity in grain identification. Each pixel in an EBSD scan is labeled with an angular orientation (simplified to a single angle for purposes of the figure; real grain orientations are three dimensional), with a random error $\sim 0.5^\circ$. A local grain-boundary-finding algorithm with a 1° threshold would identify the bold edges as grain boundaries. A global algorithm would take the output of the local algorithm and enforce minimal transitivity. Under the global algorithm, the bold edges would not be considered grain boundaries, and it is impossible for a boundary to end in the middle of a grain. The pictured situation can arise from both statistical measurement fluctuations and localized plastic deformation. Analysis of grain boundary network topology usually uses some version of the global algorithm and is typically performed on well-annealed polycrystals that rarely exhibit this problem in any case

The categorization of grain boundaries is described elsewhere in this volume and will be briefly summarized here. Suppose each grain A, B, C, . . . has its orientation represented as a rotation A, B, C, \dots (which may be a matrix, a quaternion, a Rodriguez vector, or a set of Euler angles; see Chapter 3). Then the *misorientation* is a rotation specified in the reference frame of one of the grains by, for example, $M_{AB} = A^{-1}B$ (this convention, and the alternate convention $M_{AB} = BA^{-1}$, are both widely used; either is acceptable so long as consistency is maintained).

For a given grain boundary, the misorientation is usually almost constant as a function of space and time and is typically considered a property of the *entire* grain boundary rather than of one localized piece of it at a given time. This is important, as this property is not shared by the grain boundary plane normal $\hat{n}_{AB}(\vec{r}, t)$, which can vary extremely rapidly for a highly faceted, fast evolving boundary. Thus, while it is recognized that both M_{AB} and \hat{n}_{AB} are important for the atomic structure, energy density, and mobility of a boundary, for purposes of studying the network topology the attention of the field has traditionally focused almost exclusively on M_{AB} . There is also a practical concern, as the M_{AB} are much easier to determine from EBSD scans than are the \hat{n}_{AB} (see Chapter 16 by Rohrer and Randle).

The misorientation between two adjacent EBSD pixels will fall into one of the following categories:

1. Subthreshold: smaller than the $\sim 1^\circ$ threshold described above. In this case the two pixels are part of the same grain.
2. Low-angle boundary (LAB): greater than the threshold but smaller than some moderately small angle, typically set at $\sim 15^\circ$, above which the dislocation cores making up the boundary are considered to overlap (Read and Shockley 1950).
3. Coincident-site-lattice (CSL) boundary, with M_{AB} within some acceptable error (such as the Brandon criterion [Brandon 1966] $\theta_{\max} = 15^\circ / \Sigma^{1/2}$) of a low- Σ CSL misorientation.
4. Otherwise unique or symmetric non-CSL high-angle boundary, which can occur in some materials (Lejcek and Paidar 2005; Randle 2006; Zhao et al. 1988).
5. General high-angle boundary (GHAB), i.e., anything not covered by the above categories.

For any given material, some misorientations correlate to significantly enhanced properties with respect to impurity segregation and embrittlement, cracking, coarsening, diffusion, or other properties associated with grain-boundary-mediated failure and material property degradation. These misorientations, and the boundaries that have them, are termed *special*, while other boundaries are *general*. “Special” does not necessarily mean that a boundary *does* have enhanced properties, but rather that portions of it *could* have enhanced properties, should their boundary planes fall into the right orientations.

15.2.2 Structures with More than One Boundary

A key insight of grain boundary network analysis is that often the properties of a single boundary are relevant to material performance only in the context of a network. There are two complementary ways in which the network is important. First, there are many situations in which we are concerned with, e.g., transport or damage propagation along contiguous paths of grain boundaries. These are called “direct lattice” properties. Second, many problems involve the complementary issue of transport *across* grain boundaries. Examples include electrical conductivity or superconductivity, where general boundaries are more disruptive to current flow than are special ones. These are called “dual lattice” properties, as they involve connectivity not among the grain boundaries directly, but among grain centers. A cartoon illustrating the direct and dual lattices for a hexagonal grain boundary network is shown in Fig. 15.2.

In a later section, we will clarify the connection between the structure of the boundary network, the dual network, and various properties that rely upon them. Central to understanding the structure-property connection are the rules by which grains and grain boundaries can connect together in the network. The basic elements of boundary connectivity are the *triple junctions*, the one-dimensional edges of grain boundaries where three grains and three boundaries meet; and the *quadruple nodes*, the zero-dimensional points where four grains, six boundaries, and four triple junctions meet.

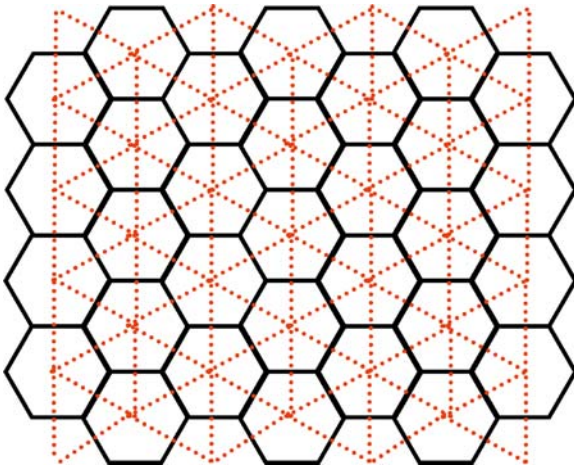


Fig. 15.2 Illustration of a hexagonal lattice (solid black lines) that represents a network of grain boundaries in a 2D section of a polycrystal, and the corresponding “dual lattice” (dashed red lines) that defines the topology of transgranular paths

Triple junctions and quadruple nodes cannot be constructed arbitrarily; they are subject to constraints (see Fig. 15.3). For example, consider the Σ combination rule (Gertsman 2001b; Miyazawa et al. 1996). If three CSL boundaries (Σ_a , Σ_b , and Σ_c) in a cubic material meet at a junction, their Σ numbers must satisfy the relation $ab = m^2c$, where m is a common factor of a and b . Thus Σ_3 - Σ_3 - Σ_9 and Σ_9 - Σ_9 - Σ_9 triple junctions are allowed, while Σ_3 - Σ_3 - Σ_3 and Σ_3 - Σ_5 -

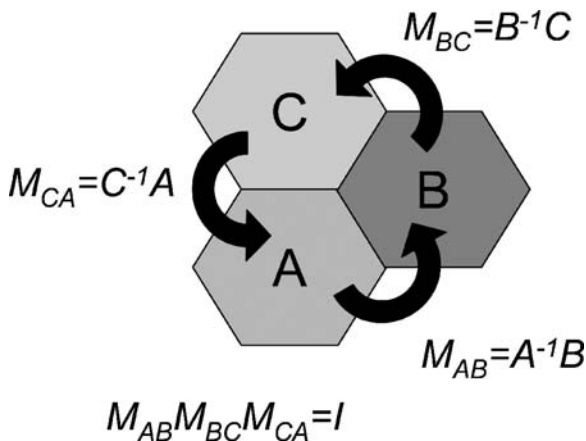


Fig. 15.3 Three grains (A, B, and C) at a triple junction with orientations A, B, and C, have a necessary connection among their misorientations M_{AB} , M_{BC} , and M_{CA} , even if the orientations themselves are completely uncorrelated. The triple junction is a triangle in the dual network of Fig. 15.2

Σ_7 triple junctions are crystallographically impossible. The rules are relaxed somewhat when deviations from the ideal cases are considered (Frary and Schuh 2003a), but the ideal CSL boundaries are rigidly constrained.

Note the immediate practical implication: The strongest boundaries in many cubic materials are the Σ_3 twin boundaries, but since it is impossible for three such boundaries to come together in a triple junction, it is impossible to make a nontrivial grain boundary network entirely out of the strongest boundaries; weaker boundaries *must* be included in the mix.

Beyond the triple junction constraint in Fig. 15.3, there are potentially an infinite number of higher-order constraints analogous to the Σ combination rule. While some of these constraints will be redundant, the examples in Fig. 15.4 show a trend: as we make the network more complex, the locally-derived constraints from one level of complexity never exactly capture all of the constraints for the next higher level. In the first row of Fig. 15.4, we see a triple junction that satisfies the Σ combination rule, yet is mathematically impossible because we have overspecified the crystallographic boundary types. In the second row, we see a quadruple node in which every triple junction is valid, yet the quadruple node is illegal (Gertsman 2001a). The third row shows a cluster of five grains in which every quadruple node is legal, yet the greater structure is disallowed (Reed et al. 2004). In short, we may identify a hierarchy of local constraints on the way that different boundary types may be combined into a network. In the next section we shall see how some of these constraints imply a degree of short- and long-range correlation in the boundary networks of real materials.

15.3 Geometry of the Network Structure

The assignment of grain boundaries as either “special” or “general” arose historically as a means of simplifying the overwhelmingly complex grain boundary network into a simple statistical description, in which the fraction of special grain boundaries becomes the essential state variable. This binary description leads naturally to the use of tools from statistical physics, most notably percolation theory, which is extremely well developed for binary systems (Grimmett 1989; Stauffer and Aharony 1994). Consequently, much of

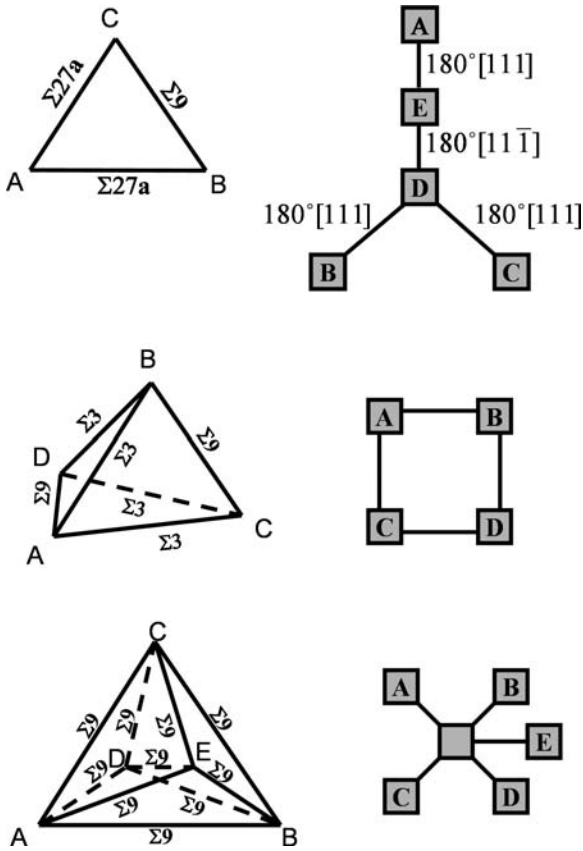


Fig. 15.4 Examples of impossible constructions in a cubic polycrystal. *Left column:* Dual network. *Right column:* $\Sigma 3^n$ connectivity diagram (each node is a potential grain orientation and each link is a single $\Sigma 3$ operation [Reed et al. 2004]). *First row:* The Σ combination rule is satisfied, but the construction is still impossible because there is no allowable assignment of specific $\Sigma 3$ operators to each link. The pictured assignment (which is forced, modulo an arbitrary choice of convention, by the $\Sigma 27a$ boundaries) fails because node D links to two different nodes (B and C) through the same $\Sigma 3$ operator. *Second row:* Even though every triple junction in the $4\Sigma 3 - 2\Sigma 9$ quadruple node satisfies the Σ combination rule, the global construction is impossible because it implies that the $\Sigma 3^n$ diagram must have a loop, which is illegal for this group. *Third row:* A cluster of five mutually-adjacent grains with all $\Sigma 9$ boundaries. Even though all of the quadruple nodes are perfectly legal, the global construction is impossible because it forces one node to have five neighbors when there are only four distinct fundamental $\Sigma 3$ operations. Adapted from Reed et al. (2004)

our understanding of grain boundary network structure is built upon the concepts of percolation theory. In this section we briefly review the standard geometrical percolation problem as it applies to grain boundary networks, focusing upon what this approach teaches

us about the clustering of grain boundaries. We then review the effects of crystallographic constraints as described previously, and how these affect the structure of grain boundary clusters and the percolation transition.

15.3.1 Percolation Measures of the Grain Boundary Network

As noted above, the basic state variable used in grain boundary percolation problems is the fraction of special boundaries in the network. Conventionally a number fraction, p , is used to appreciate the statistics of grain boundary connectivity (although EBSD software more routinely outputs a length fraction). The basic components of percolation theory include the percolation threshold and a set of scaling relationships. These can be understood most easily by considering what happens in a microstructure if we begin from a network comprising only general boundaries ($p = 0$), and progressively substitute in special boundaries (progressively increase p). For now, let us imagine that the special boundaries are placed randomly into the network.

For low values of p , the special boundaries will tend to be isolated from one another, and only rarely connect together. As p rises, gradually the special boundaries become connected into small contiguous groups, or clusters. These clusters grow in size and in topological complexity as p increases. Put another way, the average cluster radius of gyration increases, or the mean connectivity length of the special boundaries rises with p . In fact, in percolation problems it is established that the connectivity length, ξ , increases as a power-law:

$$\xi \propto (p_c - p)^{-\nu}. \quad (15.1)$$

This power law diverges to infinity at a critical value of p , called the percolation threshold, p_c . This critical point thus separates those microstructures which have an infinitely connected path of special boundaries (at high p) from those that do not (at low p). There is also a complementary power law and percolation threshold for the general boundaries, the fraction of which is $q = 1 - p$, with q_c the percolation threshold for general boundary connectivity.

Equation (15.1) is just one of many similar power-law scaling relationships that describe the statistics of grain boundary clusters and their properties. Related equations describe the distribution of cluster sizes, the strength or size of the largest percolating cluster, the fractal nature of clusters, and other statistical properties of the boundary network. Interestingly, the power-law equations that capture all of these details are considered “universal” for all geometrical percolation problems, and numerical values for the power-law exponents are known and tabulated. The power-law exponents do not change with details of the grain structure, including grain size or shape, but only with the dimensionality of the microstructure.

Grain boundary cluster statistics have been quite thoroughly studied in two dimensions. For example, Frary and Schuh (2005b) used computer simulations of various microstructures to explore percolation and scaling of special and general grain boundaries. Complementary experimental studies (Schuh et al. 2003a, 2003b) have provided software tools that analyze boundary clusters directly from EBSD datasets. Percolation, clustering, and scaling laws have also been addressed in three-dimensional simulated structures in Frary and Schuh (2005a, 2005b), and three-dimensional experimental data are also beginning to emerge (King et al. 2008).

The scaling laws and percolation threshold offer a simple statistical means of assessing how connected the special and general boundaries are in a given microstructure or family of microstructures. This has important implications for the structure-property relationship of polycrystals, as we will discuss in a later section.

15.3.2 Crystallographic Constraints

In the above discussion of percolation and scaling, it was convenient to envision grain boundary types being randomly distributed in the network. In reality, they are not randomly distributed, and in fact can never be randomly distributed by virtue of the correlations described earlier; misorientation conservation rules govern the assembly of boundary clusters. Some of the early EBSD studies of grain boundary connectivity drew attention to this specific issue, by looking

at, e.g., the coordination of special grain boundaries at triple junctions.

Figure 15.5 illustrates the so-called *triple junction distribution* for a variety of FCC metals, as measured using EBSD in Schuh et al. (2005). This plot indicates what fraction of the triple junctions, J_i , are coordinated by i special boundaries, given a special boundary fraction p . Shown for comparison are expectation curves for a boundary network assembled at random; the deviation of the experimental data from these curves illustrates the effects of crystallographic constraints on the local clustering of boundaries at their nearest-neighbor connection points.

The basic trend in Fig. 15.5 is seen repeatedly in polycrystals, even when the definition of boundary specialness is changed. For example, in networks differentiated only on the basis of low vs. high disorientation angles, a similar triple junction distribution is found (Frary and Schuh 2004). In general, it seems that crystallography tends to suppress pairs of special boundaries (J_2), in favor of triplets (J_3) or “dangling ends” (J_1). There is an intuitive reason for this: special misorientations tend to be related to one another, so that the product of two special misorientations has an enhanced probability of being special itself. Conversely, general boundaries tend to collect in pairs at triple junctions. This amounts to a bias in the types of grain boundary clusters that form in polycrystals, which is readily seen upon inspection of the network. For example, Fig. 15.6 compares two simulated grain boundary networks from Frary and Schuh (2004); the network on the left was assembled at random, without heed of crystallographic constraints, while that on the right is a realistic microstructure where the boundary types were based on misorientation calculations of the crystal orientations. In each figure, only general boundaries are shown; the assembly of these into clusters is clearly affected by the crystallographic constraints, which favor the formation of longer, stringier clusters.

Similar analyses of grain boundary clusters have led to a more sophisticated understanding of the microstructures produced by multiple twinning. Many materials exhibit simple twinning patterns, in which individual “parent” grains are segmented into parallel bands alternating between two twin-related orientations (Fig. 15.7 [a]); that is, the parent grain contains twin subgrains separated by $\Sigma 3$ twin boundaries. This kind of simple back-and-forth twinning

Fig. 15.5 Experimental data acquired by EBSD on 70 different FCC metals, including aluminum, copper, nickel, and iron alloys, showing the distribution of triple junction types in the microstructure. The value of J_i indicates the fraction of triple junctions with i special boundaries, given a special boundary fraction p . The blue solid curves show the expected trends for a network assembled at random; the deviation of the experimental data from these trendlines is an effect stemming from crystallographic constraints, which generally dictate that when two special boundaries meet at a junction, they are very likely to be mated with a third special boundary. After Schuh et al. (2005)

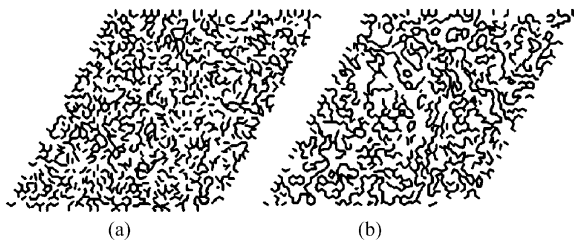
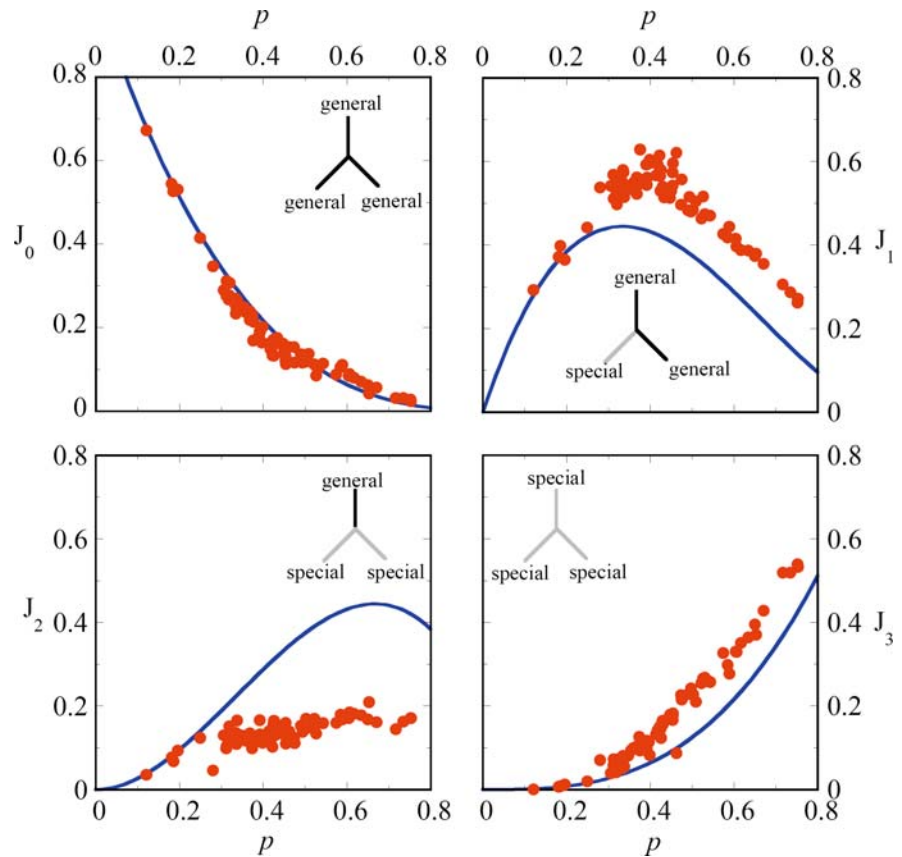


Fig. 15.6 Simulated grain boundary networks reproduced from Frary and Schuh (2005b). Both networks have 50% special boundaries ($p = 0.5$), but only the general boundaries are shown here. The network shown in (a) is random, meaning that no crystallographic constraints are enforced, while that shown in (b) enforces complete crystallographic constraints. The resulting cluster topologies are quite different, with general boundaries favoring longer and stringier clusters when crystallographic effects are included

is common in many deformation scenarios, with a strong bias towards twinning in certain orientations. While the parent grain/subgrain description is convenient for such microstructures, it becomes more awkward for the complex twin-related grain clusters that

can occur in some grain boundary engineered materials (Fig. 15.7[b]), where twinning occurs on many different boundary planes, and boundaries of type $\Sigma 81$ or higher can arise from the indirect interaction of $\Sigma 3$ misorientations. These clusters have been referred to as twin-related domains (TRDs; Reed and Kumar 2006), and they can be identified as clusters of $\Sigma 3^n$ boundaries in the dual network (Gertsman and Henager 2003; Kopecky et al. 1991). Any two grains in the TRD will have a $\Sigma 3^n$ misorientation. Usually this misorientation very closely approximates the theoretical ideal, because the TRDs typically grow from a sequence of annealing twinning events, each of which usually creates a nearly perfect $\Sigma 3$ misorientation. Conversely, the boundaries *between* TRDs are usually general, which accounts for the extended, “stringy” appearance of large general boundary clusters in these materials. The literature suggests that TRDs define a characteristic length scale in the cluster size distributions (Reed et al. 2008) and that percolation behaviors approach universality above this scale.

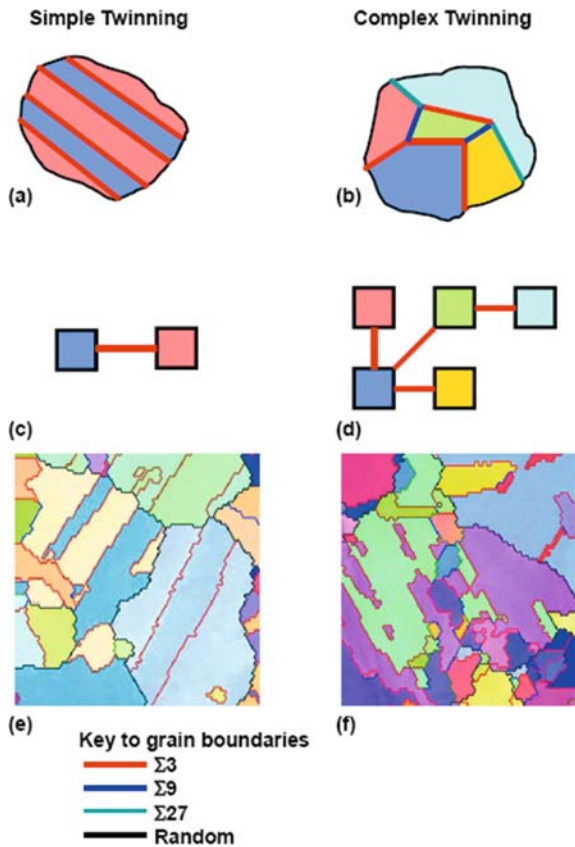


Fig. 15.7 Examples of twinned microstructures. (a) Schematic of a typical grain-subgrain geometry dominated by back-and-forth twinning on parallel $\{111\}$ planes. The associated twin subgrain boundaries generally play a negligible role in the larger network connectivity. (b) Schematic of a complex twin-related domain with each grain twinning more or less isotropically on different $\{111\}$ planes. This results in a complex intra-TRD network that can play a decisive role in breaking up the larger scale random boundary clusters. (c, d) $\Sigma 3^n$ connectivity diagram (see Fig. 15.4) for the microstructures in (a, b). The complexity of the *right hand column* is of an entirely different order. (e, f) Example EBSD inverse pole figure maps of each type of microstructure

Methods have been developed for identifying TRDs and for characterizing their internal crystallographic relationships with a simple graphical representation (Fig. 15.7[c, d]; Reed and Kumar 2006; Reed et al. 2004). In this representation, each grain orientation is a node (color coded to match the grains in Fig. 15.7[a, b]), each link is a $\Sigma 3$ misorientation, and two nodes separated by n links have a misorientation of $\Sigma 3^n$. The rules for drawing the graphs ensure that all crystallographic constraints are satisfied within the TRD.

Crystallographic constraints require some modification to the percolation-theory description of the boundary network. In general, because crystallographic constraints promote longer and stringier clusters of general boundaries, they tend to favor percolation of general boundaries at lower general boundary fractions, q . Conversely, crystallographic constraints generally lead to clumping of special boundaries in relatively compact cluster structures, which means that larger special fractions, p , are required to achieve percolation.

The percolation thresholds of grain boundary networks have been well studied both in two and three dimensions, and for different crystallographic textures, and with various definitions of boundary specialness. A recent compilation of the resulting percolation thresholds is provided by Frary and Schuh (2005a), from which Table 15.1 is taken. In general, all of these studies reveal that grain boundary networks, as compared with randomly assembled networks, require a greater fraction of special boundaries to effect percolation transitions. For practitioners of “grain boundary engineering,” this has important implications as to what special fraction, p , constitutes success in the exercise of microstructure design. This issue will be made clearer in the following section, where we discuss how the grain boundary network structure impacts the properties of polycrystals.

15.4 Microstructure-Property Connections

The connection between the grain boundary network structure and the properties of a polycrystal can generally be regarded as a composite problem, where we wish to develop a proper “average” of the properties of the grain boundaries in the network. In a simple binary classification scheme using special vs. general grain boundaries, these “average” or “effective” properties are a function of the fractions of these two species, as well as their topological arrangements. Much of the development on this topic is mathematically focused and therefore beyond our immediate scope. Instead, our purpose is to briefly highlight some of the major defining features of microstructures and their properties, and the methods used to quantitatively connect them.

Table 15.1 A compilation of percolation thresholds after Frary and Schuh (2005a) for grain boundary networks in both 2D and 3D, and with different textures and rules for boundary special-

	2D networks		3D networks	
	$q_{c,general}$	$p_{c,special}$	$p_{c,special}$	$q_{c,general}$
Randomly assembled	0.653	0.653	0.775	0.775
Fiber textured	0.601	0.689	0.711	0.842
General textured	0.676	0.663	0.818	0.835
Multiply twinned	0.659	0.666	0.789	0.801

ness. The thresholds for both special and general boundaries are listed

15.4.1 Composite Averaging vs. Percolation Theory

In the introduction, it was hinted that some properties are strongly dependent upon the topology of the grain boundary network (or the dual network), while others are more amenable to simple composite averaging schemes. The main consideration that separates these classes of properties is the *property contrast*, or the degree to which special and general grain boundaries differ in a given property. For example, there are some material/property combinations for which low- Σ boundaries differ by many orders of magnitude from their high- Σ counterparts, e.g., diffusion, diffusional sliding, or intergranular cracking rates in FCC metals (Lim and Raj 1984; Watanabe 1983). Such properties are said to have “high contrast.” Conversely, for other properties such as fatigue cracking the Σ number appears to have only a subtle effect, i.e., the system is “low contrast” (Gao et al. 2007).

In general, when properties exhibit low contrast, they are less dependent upon microstructural topology; when the properties of any two boundaries are similar, the details of how they connect have a relatively small influence on the average properties of the network. In the limit where special and general boundaries have the same properties, their relative spatial arrangements are arbitrary as far as the average system properties are concerned. Low contrast systems are thus relatively simple to model from a structure-property connection perspective, and usually quite simple effective medium approaches give remarkably reasonable results.

An example of a low contrast situation on a simple two-dimensional grain boundary network is shown in Fig. 15.8 (a), which represents a concentration gradient for simulated diffusion across a network of grain boundaries (Chen and Schuh 2006). Here the sys-

tem has about 30% special grain boundaries ($p = 0.3$), through which impurities diffuse ten times more slowly than they do through the general boundaries. The diffusivity contrast ratio of 10 is considered low, and the resulting diffusion profile is quite planar; as a result, one can easily define an average concentration gradient, and by extension an average diffusivity for the entire network. Figure 15.8(c) shows the net, or effective, diffusivity of such a network, as the fraction of special boundaries is varied over the full range. Because the contrast is low, a straightforward effective medium-type average yields an excellent fit to the data (shown by the solid line).

Because grain boundaries have such a broad range of possible structures, it is more common that they exhibit high contrast in properties. The same example from above, using a more realistic diffusivity contrast of 10^8 , reveals new complexities in the structure-property connection. Figure 15.8(b) shows the concentration profile for such a network, again given 30% slow-diffusing special boundaries ($p = 0.3$). Due to the high contrast, the concentration gradient cannot be simply described with an average plane, because the local undulations and variations across the network are of the scale of the entire gradient. This interesting effect speaks to the importance of topology: for high contrast systems, details of connectivity dominate the effective properties of the grain boundary network. In this case, effective medium models are insufficient to describe the average properties because they do not properly capture the percolation threshold of the system. The corresponding effective diffusivity of the network from Fig. 15.8(b) is shown in Fig. 15.8(d), showing a rapid change in diffusivity at the percolation threshold at $\sim 65\%$ general boundaries. For such high contrast systems, percolation theory can be used to reasonably capture the structure-property connection. Much like the geometrical properties of the grain

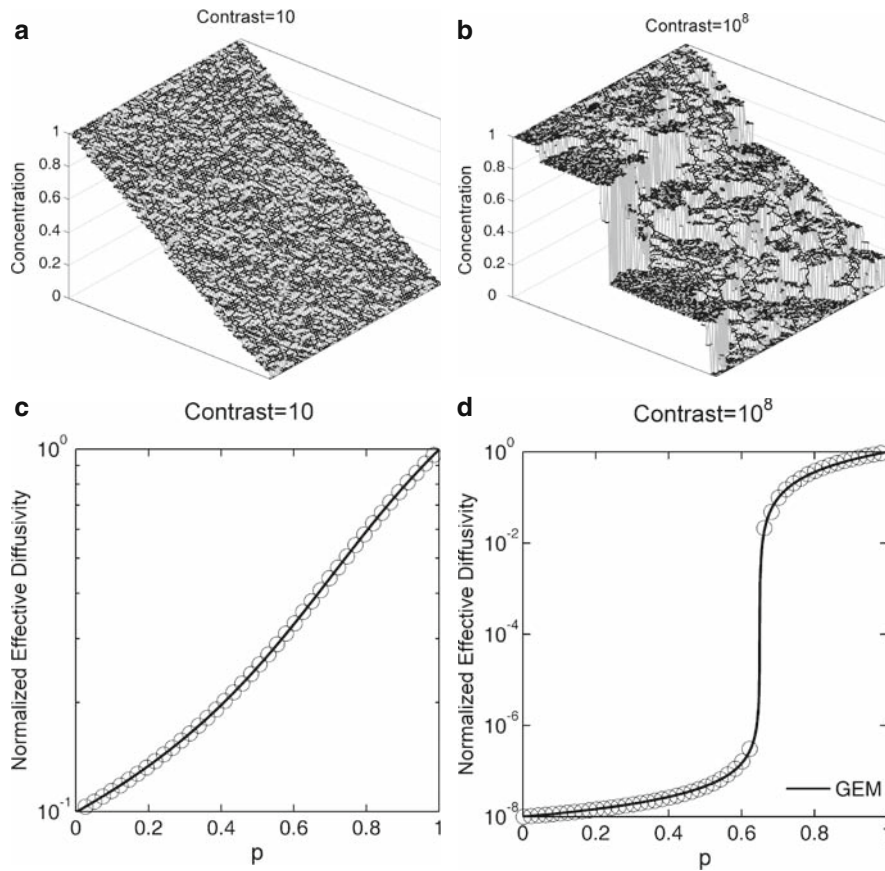


Fig. 15.8 Illustration of the role of property contrast in the structure-property relationships of polycrystals. These simulation data are from Chen and Schuh (2006), and consider intergranular diffusion on a simple 2D boundary network. In (a) and (c), the situation of low property contrast is considered, where the special boundaries are only 10 times more slowly diffusing than the general ones. As a result, the concentration gradient is on average quite linear (a), and the effective diffusivity of the

network varies smoothly with the special boundary fraction, p (c). In (c) the predictions of standard effective medium theory are shown as a *solid line*, and match the simulations quite well. In (b) and (d), the high contrast case is shown, for which the situation is less well behaved and the effect of a percolation threshold is seen. In (d) the line shown is the prediction of a generalized effective medium theory that incorporates a percolation threshold. After Chen and Schuh (2006)

boundary clusters described earlier, the physical properties also generally scale as power laws in $(p-p_c)$, and equations taking the form of Eq. (15.1) generally describe the effective properties of networks with excellent accuracy.

The introduction of percolation concepts into grain boundary network analysis provides a necessary conceptual underpinning for the practice of grain boundary engineering. As noted earlier, for many properties including intergranular cracking and corrosion, superconductivity, and creep, “grain boundary engineered” materials often exhibit improved properties by large margins (e.g., up to orders of magnitude) as compared

with nonengineered counterparts of the same composition (Krupp et al. 2003, 2005; Lehockey et al. 1998a, 1998b; Michiuchi et al. 2006; Shimada et al. 2002; Spigarelli et al. 2003). As suggested by Fig. 15.8(d), grain boundary engineering can be so remarkably effective because of the presence of a percolation threshold; a small change in microstructure (an increase in the fraction of special boundaries) can yield a large property change only in the vicinity of the threshold, for a high contrast system. In short, grain boundary engineering permits one to shut down long-range damage pathways, or open long-range conduction pathways, through microstructures.

A beautiful mathematical feature of percolation theory is that the direct and dual lattices are intimately related, and understanding percolation on one of these is tantamount to understanding it on both. In two-dimensional situations in particular, the percolation thresholds are simply complementary, i.e., $p_c^{direct} + p_c^{dual} = 1$. Thus, there is great generality in grain boundary network studies; those that study an intergranular process are relevant to transgranular properties, and vice versa.

The question remains as to how to identify the high and low contrast regimes, and how to handle systems intermediate to these two limiting cases. Figure 15.9 shows the general effect of contrast on the structure-property relationship, as studied for the case of diffusion in two-dimensional networks in Chen and Schuh (2006). Here the goodness-of-fit (R^2) of analytical models based on effective medium theory and percolation theory to numerical simulation data are presented. The main point of this graph is the complementary nature of these two modeling approaches: for low contrast systems, topology is apparently unimportant and the effective medium theory is exact; while at high contrast, topology dominates the problem and the scaling laws of percolation theory become essentially

exact. Outside of these regimes, either theory quickly loses accuracy. Figure 15.9 can be used as a general guideline for the choice of a model to connect structure and properties in GB networks.

For the intermediate range, there are some proposed models that combine percolation theory with more traditional composite averaging schemes to provide a structure-property prediction that spans all possible property contrast ratios. One example that has proven valuable for simulated grain boundary networks is the so-called generalized effective medium (GEM) theory of Mclachlan (1987). This model empirically adapts the effective medium theory to incorporate the percolation threshold and critical scaling exponents of percolation theory. As shown in Fig. 15.9, such a model can be quantitatively descriptive for virtually any grain boundary network. Further, this type of model can be extended beyond the simple binary “special” vs. “general” approach to include a broader spectrum of grain boundary types. In Chen and Schuh (2006), the GEM model was extended to an arbitrary number of different grain boundary types, and validated against simulations on ternary grain boundary networks.

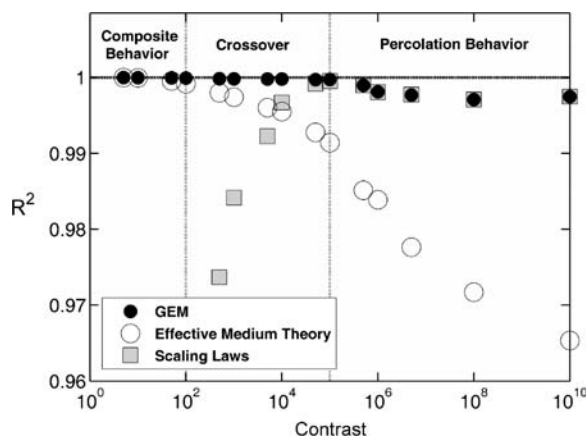


Fig. 15.9 The general effect of property contrast on the structure-property relationships of grain boundary networks, showing the coefficient of determination, R^2 , which describes the degree of accuracy with which a given model represents the true effective properties of a network. At low contrast, simple effective medium theories (composite averages) are remarkably accurate; while at high contrast, percolation theory scaling equations are more useful. Generalized effect medium theories (GEM) combine features of both models and capture both types of behavior, at all contrast levels. After Chen and Schuh (2006)

15.4.2 Crystallographic Correlations

The crystallographic correlations described at length above tend to shift the percolation threshold by promoting connectivity among special grain boundaries. Fortunately, however, these correlations are short-range, and they do not alter the critical scaling laws associated with percolation (Frary and Schuh 2005b). This is good news for modeling the structure-property connection, because although the specific numerical value of the percolation threshold shifts due to crystallographic effects, the shapes of the effective property curves are unchanged. An example of this is illustrated in Fig. 15.10 for the case of grain boundary diffusional creep, from Chen and Schuh (2007). Here the effective creep viscosity is plotted for both a randomly assembled network and one with proper crystallographic correlations. Although the percolation threshold is different, the same scaling laws apply near the threshold (i.e., the same curvatures are present in the sigmoid), and the same analytical model can be used to describe both curves.

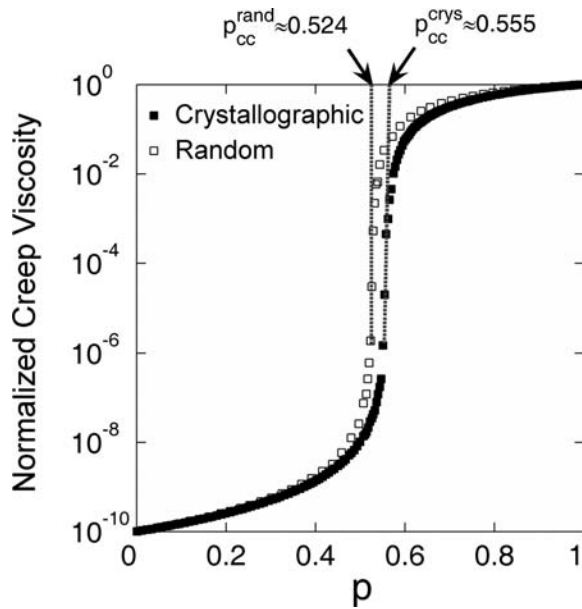


Fig. 15.10 Example of percolation data for grain boundary networks, illustrating the role of crystallographic constraints. These data for Coble (diffusional) creep are from computer simulations on 2D hexagonal grain boundary networks. The effect of crystallographic constraints is to shift the percolation threshold somewhat, but the shapes of the curves (and the exponents of the power laws that describe them) are unchanged. After Chen and Schuh (2007)

15.5 Conclusions and Future Outlook

The field of grain boundary network analysis is moving quickly; not many years ago, there were very few practitioners in this particular subfield, but there seems to be a growing realization about the importance of correlated percolation in the performance of a material. Thus we conclude with a few observations about the possible future course of the field:

- Most published experimental studies of grain boundary network statistics rely exclusively on two-dimensional cross sections via EBSD. Yet the boundary networks in most materials are irreducibly three-dimensional, which introduces significant complexity. Advances in serial sectioning and digital reconstruction techniques, as well as advanced X-ray diffraction methods, now permit access to fully three-dimensional data sets com-

pletely describing the grain structure of a material. Percolation problems change subtly going from two to three dimensions; it is quite possible that both the special boundaries and the general boundaries may percolate over a very wide range of special boundary fractions. The three-dimensional structure of twin-related domains also remains somewhat mysterious, and could be elucidated with such new tools.

- Early in this chapter we introduced a classification scheme for grain boundaries, much as the field has always done in order to simplify the description of the boundary network. Future advances in this field will rely upon progressively adding more details to this classification scheme, including boundary plane inclinations, orientation of boundaries with respect to, e.g., an external stress axis, and thermodynamic state variables such as the degree of boundary relaxation. Although some of the effective medium type modeling approaches laid out in this chapter can be extended from the binary case to include more differentiation in boundary properties, there is a significant experimental challenge to assess connectivity among boundaries that are not merely special or general, but which lie on a multidimensional spectrum of structure and properties.
- Whereas some properties are primarily concerned with connectivity on the direct lattice (intergranular pathways) and others are more appropriately treated on the dual (transgranular paths), many properties involve both lattices simultaneously. For example, stress corrosion cracking is one of the best-known examples of a property that can be manipulated broadly through grain boundary engineering, and it implicitly involves intergranular damage propagation coupled to a force transmission network across the grain boundaries. In percolation theory correlated problems are relatively common, but correlations between direct and dual lattices are essentially unstudied. The aims of the materials science community therefore require study of this new statistical physics problem.

These problems represent some of the most immediate needs of the community working on grain boundary networks. As always, access to improved experimental tools based on EBSD will drive continued progress on these problems.

References

- Basinger JA, Homer ER, Fullwood DT, Adams BL (2005) Two-dimensional grain boundary percolation in alloy 304 stainless steel. *Scripta Mater* 53(8):959–963
- Bouchaud E (1997) Scaling properties of cracks. *J Phys-Condens Mat* 9(21):4319–4344
- Brandon DG (1966) Structure of high-angle grain boundaries. *Acta Metall* 14(11):1479
- Chen Y, Schuh CA (2006) Diffusion on grain boundary networks: Percolation theory and effective medium approximations. *Acta Mater* 54(18):4709–4720
- Chen Y, Schuh CA (2007) Coble creep in heterogeneous materials: The role of grain boundary engineering. *Phys Rev B* 76(6):064111
- Frary M, Schuh CA (2003a) Combination rule for deviant CSL grain boundaries at triple junctions. *Acta Mater* 51(13):3731–3743
- Frary M, Schuh CA (2003b) Nonrandom percolation behavior of grain boundary networks in high-T-c superconductors. *Appl Phys Lett* 83(18):3755–3757
- Frary M, Schuh CA (2004) Percolation and statistical properties of low- and high-angle interface networks in polycrystalline ensembles. *Phys Rev B* 69(13):134115
- Frary M, Schuh CA (2005a) Connectivity and percolation behaviour of grain boundary networks in three dimensions. *Philos Mag* 85(11):1123–1143
- Frary M, Schuh CA (2005b) Grain boundary networks: Scaling laws, preferred cluster structure, and their implications for grain boundary engineering. *Acta Mater* 53(16):4323–4335
- Fullwood DT, Basinger JA, Adams BL (2006) Lattice-based structures for studying percolation in two-dimensional grain networks. *Acta Mater* 54(5):1381–1388
- Gao Y, Stolken JS, Kumar M, Ritchie RO (2007) High-cycle fatigue of nickel-base superalloy Rene 104 (ME3): Interaction of microstructurally small cracks with grain boundaries of known character. *Acta Mater* 55(9):3155–3167
- Gaudett MA, Scully JR (1994) Applicability of bond percolation theory to intergranular stress-corrosion cracking of sensitized A1s1 304 stainless-steel. *Metall Mater Trans A* 25(4):775–787
- Gertsman VY (2001a) Coincidence site lattice theory of multicrystalline ensembles. *Acta Crystallogr A* 57:649–655
- Gertsman VY (2001b) Geometrical theory of triple junctions of CSL boundaries. *Acta Crystallogr A* 57:627–627
- Gertsman VY, Henager CH (2003) Grain boundary junctions in microstructure generated by multiple twinning. *Interface Sci* 11(4):403–415
- Grimmett G (1989) *Percolation*. Springer-Verlag, New York
- King A, Johnson G, Engelberg D, Ludwig W, Marrow J (2008) Observations of intergranular stress corrosion cracking in a grain-mapped polycrystal. *Science* 321(5887):382–385
- Kopecky CV, Andreeva AV, Sukhomlin GD (1991) Multiple twinning and specific properties of Sigma = 3n boundaries in FCC crystals. *Acta Metall Mater* 39(7):1603–1615
- Krupp U, Kane WM, Liu XY, Dueber O, Laird C, McMahon CJ (2003) The effect of grain-boundary-engineering-type processing on oxygen-induced cracking of IN718. *Mater Sci Eng A* 349(1–2):213–217
- Krupp U, Wagenhuber PEG, Kane WM, McMahon CJ (2005) Improving resistance to dynamic embrittlement and intergranular oxidation of nickel based superalloys by grain boundary engineering type processing. *Mater Sci Tech* 21(11):1247–1254
- Lehockey EM, Palumbo G, Lin P (1998a) Improving the weldability and service performance of nickel- and iron-based superalloys by grain boundary engineering. *Metall Mater Trans A* 29(12):3069–3079
- Lehockey EM, Palumbo G, Lin P, Brennenstuhl A (1998b) Mitigating intergranular attack and growth in lead-acid battery electrodes for extended cycle and operating life. *Metall Mater Trans A* 29(1):387–396
- Lejcek P, Paidar V (2005) Challenges of interfacial classification for grain boundary engineering. *Mater Sci Tech* 21(4):393–398
- Lim LC, Raj R (1984) Effect of boundary structure on slip-induced cavitation in polycrystalline nickel. *Acta Metall* 32(8):1183–1190
- McGarrity ES, Duxbury PM, Holm EA (2005) Statistical physics of grain-boundary engineering. *Phys Rev E* 71(2):026102
- Mclachlan DS (1987) An equation for the conductivity of binary-mixtures with anisotropic grain structures. *J Phys C* 20(7):865–877
- Meinke JH, McGarrity ES, Duxbury PM, Holm EA (2003) Scaling laws for critical manifolds in polycrystalline materials. *Phys Rev E* 68(6):066107
- Michiuchi M, Kokawa H, Wang ZJ, Sato YS, Sakai K (2006) Twin-induced grain boundary engineering for 316 austenitic stainless steel. *Acta Mater* 54(19):5179–5184
- Miyazawa K, Iwasaki Y, Ito K, Ishida Y (1996) Combination rule of Sigma values at triple junctions in cubic polycrystals. *Acta Crystallogr A* 52:787–796
- Nichols CS, Cook RF, Clarke DR, Smith DA (1991a) Alternative length scales for polycrystalline materials 1. Microstructure evolution. *Acta Metall Mater* 39(7):1657–1665
- Nichols CS, Cook RF, Clarke DR, Smith DA (1991b) Alternative length scales for polycrystalline materials 2. Cluster morphology. *Acta Metall Mater* 39(7):1667–1675
- Randle V (2004) Twinning-related grain boundary engineering. *Acta Mater* 52(14):4067–4081
- Randle V (2006) “Special” boundaries and grain boundary plane engineering. *Scripta Mater* 54(6):1011–1015
- Read WT, Shockley W (1950) Dislocation models of crystal grain boundaries. *Phys Rev* 78(3):275–289
- Reed BW, Kumar M (2006) Mathematical methods for analyzing highly-twinned grain boundary networks. *Scripta Mater* 54(6):1029–1033
- Reed BW, Kumar M, Minich RW, Rudd RE (2008) Fracture roughness scaling and its correlation with grain boundary network structure. *Acta Mater* 56:3278–3289
- Reed BW, Minich RW, Rudd RE, Kumar M (2004) The structure of the cubic coincident site lattice rotation group. *Acta Crystallogr A* 60:263–277
- Romero D, Martinez L, Fionova L (1996) Computer simulation of grain boundary spatial distribution in a three-dimensional polycrystal with cubic structure. *Acta Mater* 44(1):391–402
- Schuh CA, Frary M (2006) Correlations beyond the nearest-neighbor level in grain boundary networks. *Scripta Mater* 54(6):1023–1028

- Schuh CA, Kumar M, King WE (2003a) Analysis of grain boundary networks and their evolution during grain boundary engineering. *Acta Mater* 51(3):687–700
- Schuh CA, Kumar M, King WE (2003b) Connectivity of CSL grain boundaries and the role of deviations from exact coincidence. *Z Metallkd* 94(3):323–328
- Schuh CA, Kumar M, King WE (2005) Universal features of grain boundary networks in FCC materials. *J Mater Sci* 40(4):847–852
- Schuh CA, Minich RW, Kumar M (2003c) Connectivity and percolation in simulated grain-boundary networks. *Philos Mag* 83(6):711–726
- Schwartz AJ, King WE, Kumar M (2006) Influence of processing method on the network of grain boundaries. *Scripta Mater* 54(6):963–968
- Shimada M, Kokawa H, Wang ZJ, Sato YS, Karibe I (2002) Optimization of grain boundary character distribution for intergranular corrosion resistant 304 stainless steel by twin-induced grain boundary engineering. *Acta Mater* 50(9):2331–2341
- Spigarelli S, Cabibbo M, Evangelista E, Palumbo G (2003) Analysis of the creep strength of a low-carbon AISI 304 steel with low-Sigma grain boundaries. *Mater Sci Eng A* 352(1–2):93–99
- Stauffer D, Aharony A (1994) *Introduction to percolation theory*, rev 2nd ed. Routledge, London
- Van Siclen CD (2006) Intergranular fracture in model polycrystals with correlated distribution of low-angle grain boundaries. *Phys Rev B* 73(18):184118
- Watanabe T (1983) Grain-boundary sliding and stress-concentration during creep. *Metall Trans A* 14(4):531–545
- Wells DB, Stewart J, Herbert AW, Scott PM, Williams DE (1989) The use of percolation theory to predict the probability of failure of sensitized, austenitic stainless-steels by intergranular stress-corrosion cracking. *Corrosion* 45(8):649–660
- Zhao JW, Koontz JS, Adams BL (1988) Intercrystalline structure distribution in alloy 304 stainless-steel. *Metall Trans A* 19(5):1179–1185